Measuring temperature of emulsion and immiscible two-component drops until micro-explosion using two-color LIF

Pavel Strizhak, Roman Volkov, Omar Moussa, Dominique Tarlet, Jérôme Bellettre

Measuring temperature of emulsion and immiscible two-component drops until micro-explosion using two-color LIF

Pavel Strizhak[1*], Roman Volkov[1], Omar Moussa[2], Dominique Tarlet[2], Jérôme Bellettre[2]

[1]National Research Tomsk Polytechnic University, Heat Mass Transfer Simulation Laboratory, Russia, 30, Lenin Avenue, Tomsk, 634050, Russia. +7(3822)701-777, ex. 1910

[2]Laboratoire de Thermique et Énergie de Nantes (LTeN), CNRS UMR 6607, Université de Nantes, Rue Christian Pauc, BP 50609, 44306 Nantes cedex 3, France.

*E-mail: pavelspa@tpu.ru

Abstract

In this research, we measure the temperatures of the non-combustible component (water) in a fuel droplet by 2-Color LIF before its micro-explosive fragmentation. We use two types of droplets based on water and tetradecane: a two-component immiscible droplet with water in the core and tetradecane as the envelope; a pre-mix emulsion. In both cases, the relative volume fraction of water in a droplet is 9%, and that of the combustible component (tetradecane) is 91%. To provide the micro-explosive dispersion of droplets, we use a scheme with the conductive heating in the range of 250 °C to 550 °C. Using the high-speed 2-Color LIF technique, we observe the coalescence of water micro-droplets in emulsion droplets and intense disruption of the water core in a two-component droplet when heated. The temperature difference may range from 1 °C to 10 °C. Temperature distributions in emulsion droplets are more monotone when heated until micro-explosion. In the puffing regime, the droplet temperature is 1–3 °C higher than in the micro-explosion regime at the same temperatures of the heated metal substrate surface. Within a certain interval of the heating time, the temperatures of water in a two-component droplet and in an emulsion droplet become comparable.

Keywords: micro-explosion; two-component droplet; emulsion; temperature of water; 2-Color LIF.

Nomenclature

R_d – two-component droplet radii (mm);

t – time (s);

t_d – mean droplet disintegration time (s);

Δt – time interval (s);

T_{AT} – Average Temp. value (°C);

T_{BT} – Bottom Temp. value (°C);

T_{br} – arbitrary temperature of an area without Rhodamine B on a frame (°C);

T_d – droplet temperature (°C);

T_{surf} – heating surface temperature (°C);

ΔT_d – difference between Bottom Temp. and Average Temp. of a droplet (°C);

ΔT_{AT} – variation of the mean Average Temp. value over the time interval Δt (°C);

W_h – droplet heating rate (°C/s).

Abbreviations

LIF – Laser Induced Fluorescence;

LIP – Laser Induced Phosphorescence;

PLIF – Planar Laser Induced Fluorescence.

1. Introduction

Reliable liquid droplet temperature recording is important for a wide range of activities including firefighting, evaporative cooling, heat carrier production, fuel spraying, *etc*. [1-5]). This data can be used to predict liquid heating and evaporation rates [6], thus improving the corresponding technologies. The temperature recording methods came a long way from the simplest expansion thermometers to non-contact measurement. For instance, panoramic optical methods of non-contact temperature measurement of various media have become widely popular over the last several years [7–24]. The most widespread of those are Laser Induced Phosphorescence (LIP) [8–15] and Laser Induced Fluorescence (LIF) [16–25]. Both groups of methods are based on fluorophores and luminophores' ability to absorb and emit laser radiation. The intensity of light emitted by a fluorophore depends on the temperature of the medium it was added to. As a rule, the maximum of the fluorophore emission spectrum shifts relative to the maximum of the absorption spectrum towards higher values. This makes it possible to single out the necessary wavelength using a bandpass filter. Although these methods imply adding some agents to the medium under study, they can be arbitrarily classified as noninvasive measurements. The latter is one of the reasons why they are used so actively today.

Some research findings [8–15] describe the achievements in LIP used for liquid temperature measurement. For instance, some of the authors proved the possibility to record the temperature of single free-falling water and methanol droplets [9, 10]. Omrane et al. [11] measured the temperature of an evaporating water-acetone droplet and went on to describe the methods used and results obtained. LIP is used to determine temperature distributions in liquid flows and continuous media [12, 13]. It can also be used to obtain the temperature fields of aerosol flows [14]. However, despite all of its advantages, LIP can only give a good result if particles are relatively evenly distributed throughout the medium under study. In the case of fast-paced processes and small droplet sizes [11], the particle concentration may be too low for reliable measurements. Moreover, the temperature fields obtained by LIP are often highly inhomogeneous [11, 13]. In this case, most scientists choose LIF [16–25]. The distinguishing feature of the group of methods known as LIF measurements is the complete even dissolution of the dye in the medium under study (liquid). This, in turn, solves the problem of the highly inhomogeneous temperature

fields. Generally, there are two types of LIF methods. The first type only uses the central part of the emission spectrum for recording the temperature distributions, for instance [6, 16–19], (LIF technique). In the second type, temperature is determined by the intensity ratio of the central part and the right side of the fluorophore emission spectrum, for instance [20–25], (2-Color LIF technique). LIF provides satisfactory results when obtaining the three-dimensional temperature fields of liquid flows and films, as well as large single droplets [6, 16–19]. However, it does have a number of limitations including the variations of fluorophore concentration in the measurement area [16]. Thus, without the fluorophore concentration adjustment (see [16] for a detailed description), it can be used almost exclusively at the stages of droplet heating and moderate evaporation [6, 17, 19, 20]. 2-Color LIF [21-25] prevents this, because the effect of fluorophore concentration on the intensity ratio is negligible. Moreover, the measurement results by 2-Color LIF are minimally affected by the laser beam power. Thus, 2-Color LIF is the best choice during the intense heating, evaporation, and explosive breakup of a heterogeneous droplet. Moreover, research findings have been published [25] obtained using this technique.

The study of explosive dispersion (micro-explosion) of heterogeneous multi-component droplets is a popular research field. The analysis of the recent publications (for instance, [25–33]) has shown that micro-explosion requires two-component droplets as a necessary element. It was experimentally established that micro-explosion occurs with both emulsions [28–31] and with a heated immiscible droplet [32–35]. Micro-explosion can be provided by a conductive [28–31], convective [32, 33], and radiative [34–37] heat exchange, as well as mixed mechanisms thereof. Earlier research findings [25–37] show that the threshold temperature at the interface between the combustible and non-combustible components in a droplet is the parameter that can be used to establish the patterns of micro-explosive droplet fragmentation. For instance, the threshold water temperature before the explosive dispersion is 60–80 °C for a water-in-oil droplet and 80–100 °C for a water-in-kerosene droplet [32]. Immediately before the micro-explosion, the temperature at the *water / combustible liquid* interface reaches 102–115 °C [32]. Threshold temperatures for emulsions [28–31] and immiscible compositions [32–35] are highly variable. Water droplets are observed to redistribute within the combustible component [25], which is the coalescence of the water phase known as generally leading to a successful micro-explosion [26]. Such a successful micro-explosion is different from what is called "puffing", i.e. a partial fragmentation of the drop [27, 28].

Moreover, the temperature within a droplet may be highly dependent on the heating scheme [32–41]. That is why all studies of such kind require specialized equipment and data processing algorithms. As it follows from the earlier analysis, 2-Color LIF is the technique of choice in this case [20–25]. It is also important to select the optimal droplet heating scheme for these conditions. The analysis of various heating schemes [39, 40] indicates that conductive heating (using a heated surface) is the optimal scheme for 2-Color LIF as compared to other heat exchange schemes. Radiative heating complicates the optical access to a droplet. The use of a holder in the case of radiative and convective heating is not always

acceptable, because a droplet may move in the recording area or drop off the holder due to the intense mixing of layers in the droplet and its boiling.

The purpose of this work is to experimentally study the temperatures of emulsion droplets and two-component droplets undergoing a micro-explosive breakup. It is important to observe the water location and temperature in the fuel using 2-Color LIF, to compare the coalescence of the water phase within both emulsion and two-component drops [25,26].

2. Materials

The liquid part of heterogeneous fuel-water droplets consisted of tetradecane ($CH_3(CH_2)_{12}CH_3$) and tap water with the Rhodamine B fluorophore ($C_{28}H_{31}ClN_2O_3$) (in a mass concentration of 3 g/l) [25]. Experiments were conducted for two types of droplets: two-component immiscible droplets [36–39] and emulsion droplets [32–35]. In both cases, a droplet contained 9% of water and 91% of the combustible component (tetradecane). The main properties of the combustible component (Sigma-Aldrich, No. 172456) were as follows: refractive index – 1.429; boiling temperature – 252–254 °C; density – 0.762 g/mL at 20 °C.

At the first stage, we prepared a solution of water and Rhodamine B. Rhodamine B crystals in the necessary amount were weighed on a laboratory micro-balance (with an increment of 0.0001 g) and added to water in a tank. Rhodamine B was then mixed with water for 10 min using an automatic mixer (VMS-C4). The initial temperature of the sessile droplet was about 25±1 °C.

A droplet of a two-component emulsion was prepared in the following way:

(i) using an automatic mixer (VMS-C4), we continuously mixed a water solution of Rhodamine B with tetradecane;

(ii) in the course of mixing, the emulsion was sampled by a single-channel micro-dispenser generating 2.5–50-μl droplets with an increment of 0.1 μl;

(iii) the same micro-dispenser generated a droplet of about 5.5 μl (the droplet radius approximated 1.1 mm), which was placed on a metal substrate.

A two-component immiscible droplet was prepared in the following way:

(i) using a single-channel micro-dispenser generating 2.5–50-μl droplets with an increment of 0.1 μl, we generated a tetradecane droplet with a volume of 5 μl, which was fixed on a thin steel holder, 0.6 mm in diameter;

(ii) using another (similar) single-channel micro-dispenser, we generated a droplet of a Rhodamine B water solution with a volume of 0.5 μl, which was then added to the earlier generated droplet of tetradecane;

(iii) an immiscible two-component droplet (R_d≈1.1 mm) was discharged from the holder to the metal substrate.

3. Experimental technique

The experimental setup consisted of the following main elements (Fig. 1): continuous-wave Spectra-Physics Millennia eV laser with the output power of 10 W and wavelength of 532 nm; high-speed video camera Photron FASTCAM SA-X2 (1024×1024 pix at 12,500 fps); a set of two optical lenses to transform a laser beam into a light sheet for droplet cutting; metal substrate with a cavity for the fixation of a droplet under study; TDK-Lambda Z320-1.3-U power supply delivering the current to the heating element fixed under the substrate and transferring the thermal energy to it. The droplet holder is made in aluminum and is conceived in circular convex geometry (6 mm diameter) to trap the droplet during heating process, avoiding at maximum the lateral displacement and, eventually, the droplet fall (Fig. 2). An image splitter (CAIRN Research Optosplit II) duplicates the beam from the subject to be recorded. It was equipped with a 580–600-nm dichroic mirror as well as two color filters to single out the necessary wavelength in each recording channel: 580±5 nm and 620±5 nm).

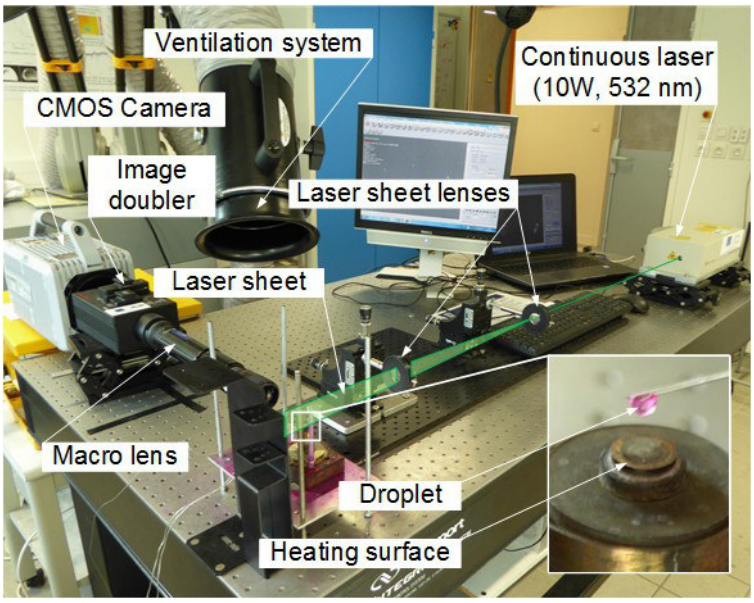

a

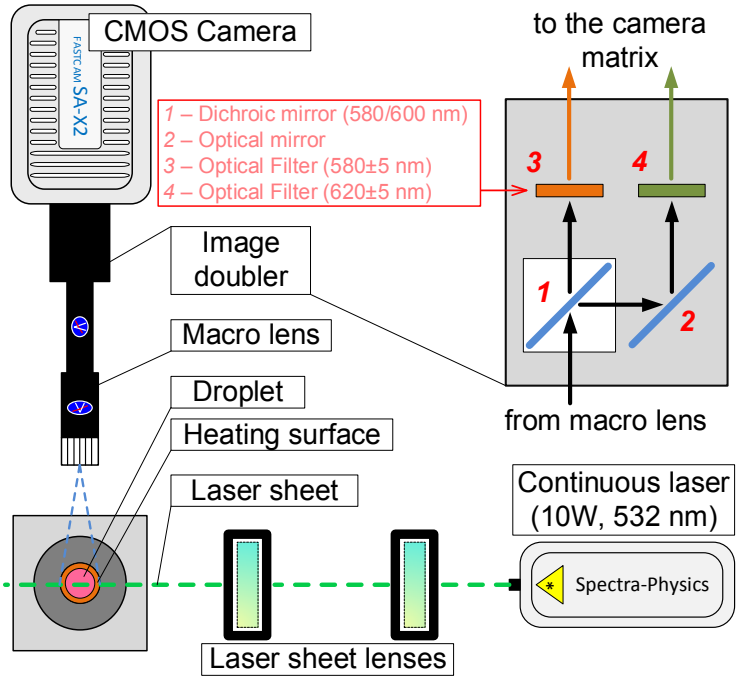

b

Fig. 1. The appearance (*a*) and layout (*b*) of the experimental setup.

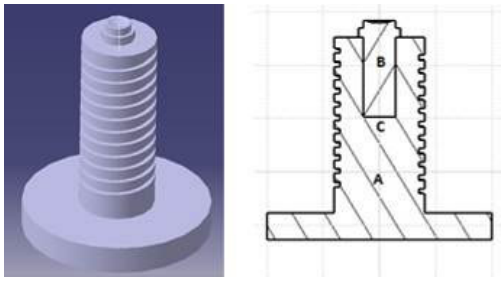

Fig. 2. Threaded support for the hot wire (A); Droplet holder (B); Position of the 80μm K-type thermocouple (C).

Each experiment was conducted in several consecutive stages:

(i) using a TDK-Lambda Z320-1.3-U, we supplied the required current to the heating element to achieve the necessary temperature (T_{surf}=150–550 °C) on the metal substrate;

(ii) a laser generated a beam, which was converted into a light sheet by a system of two lenses; the light sheet, whose thickness is around 150 μm, cuts the area above the substrate along its vertical axis (Fig. 1). The power of the laser beam is ranging between 5 and 10 W;

(iii) the processes above the metal substrate were recorded by a high-speed video camera with a frame rate of 5000 fps, exposure time of 1/8000 s, and resolution of 612×612 pix;

(iv) the resulting droplet (see stage 2) was discharged onto the substrate;

(v) the process was recorded using the Photron FASTCAM Viewer software package until the moment of droplet destruction in the micro-explosion or puffing regimes.

The resulting videos were saved as a set of consecutive frames, with a scale factor of 0.0285 mm/px. The physical size of the original image (with a camera resolution of 612 × 612 px) was about 17.44 × 17.44 mm. Due to the use of Image Doubler (Fig. 1), each frame consisted of two parts (sized 306×612 pix): the left (580±5 nm) and right (620±5 nm) channels, having dimensions of about 8.72 × 17.44 mm each. The resulting final pairs of images were imported into the DaVis software package.

The data was further processed (as exemplified by one experiment) in several consecutive stages:

(i) The image pair was geometrically corrected (droplet images from the left (580 nm) and right (620 nm) channels were aligned) using a flat calibration target with the coplanar vector arrangement, which was obtained during the system tuning; the marker was 1 mm in diameter and the distance between the centers of markers was 1.5 mm (*Image Correction*).

(ii) We analyzed the temporal variations in the average intensity of the image background. As a rule, the average background intensity in the images varied around an experiment-specific constant. The mean background intensity obtained was subtracted from each image (*Image Arithmetic*).

(iii) The luminosity ratio was determined for each pixel in the image pair (580/620 nm). As a result, we obtained one droplet image at each moment of time with the luminosity of each droplet as a

function of the liquid temperature (*Two Color LIF*). This technique is practiced as already detailed in [16,18,25,29].

(iv) The image luminosity obtained at the previous step was converted into temperature using the calibration curve equation. The hereby used calibration process is precisely described in paragraph 3 of [29], using a droplet of water mixed with Rhodamine B placed in a fixed-temperature silicone oil. First, video frames of the water droplet were recorded at various temperatures of silicone oil, assuming that the temperatures of the drop of water and silicone oil (measured by means of a thermocouple) are comparable. Secondly, the sequence of operations was performed, which is described in detail in the "data processing" section in paragraphs (i) - (iii). After that, the found values of the Fluorescence Ratio (*Rf*) were compared with the previously obtained values of the water temperature, resulting in a calibration curve $Rf=f(T)$ in the form of a second-order polynomial: $Rf=-9\cdot10^{-5}\cdot T-0.0063\cdot T+2.8499$. This way we obtained a two-dimensional temperature field of a droplet (*LIF Temperature Calculation*). If the Ratio obtained (580/620 nm) went beyond the calibration curve, this point was not assigned a temperature value.

(v) The resulting temperature field was smoothed to obtain a uniform picture (*3×3 Smoothing Filter*). More precisely, the final temperature of each pixel in the image is the arithmetic average of the 9 around pixels, which neutralizes the erroneous peaks (highs and lows) of the temperature in the final distribution.

After processing all the images, we found the temporal variation in the average droplet temperature (Average Temp.) and the temperature of the lower part of the droplet (Bottom Temp.). The Bottom Area dimensions affect the value of Bottom Temp determined by analyzing the experimental results. In most experiments, the height of a sitting droplet varied, usually in the range of 1.5-2 mm. The Bottom Area height was chosen so that it did not exceed 10% of the total droplet height, which was approx. 0.15 mm. Fig. 3 schematically depicts the areas used for the calculations of the above temperatures. As part of the calculation, we averaged the droplet temperature (*Average Processing*) at each point of time: we determined the arithmetic mean of the temperatures of all the points in the highlighted area. After that, we plotted a temperature variation curve in the highlighted area over time (Fig. 4).

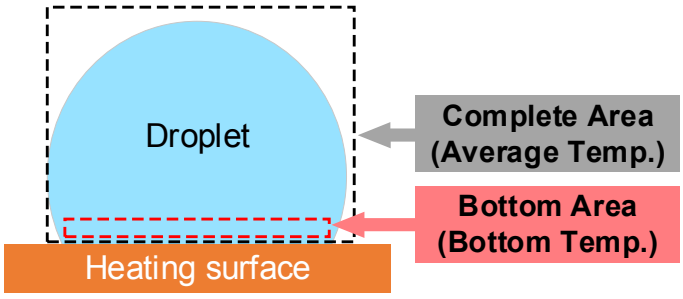

Fig. 3. Averaging areas used to determine the average droplet temperature (Average Temp.) and bottom (Bottom Temp.) part of the droplet.

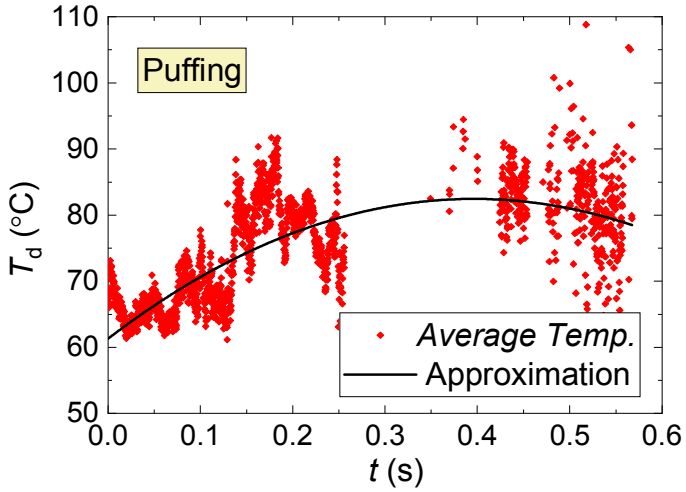

Fig. 4. Example of the average temperature variation in a two-component droplet over time at T_{surf}≈200 °C for the *puffing* regime.

Due to the re-reflection of the laser beam from the droplet and substrate, the background intensity in some frames exceeded the average value obtained at stage (ii). That is why the temperatures T_{br} were detected even in the area that did not contain the Rhodamine B fluorophore. This required plotting a curve describing the temporal variation in the average temperature T_{br}. After that, we obtained the difference T_d–T_{br} for each moment of time. At T_d–T_{br}<20 °C, experimental points were excluded from consideration; they are the white areas in Fig. 7. Then we calculated the time-average droplet temperatures (Average Temp.) and temperatures in its lower part (Bottom Temp.) for each temperature of the heated surface (T_{surf}): $T_d=(T_{d1}+T_{d2}+\ldots+T_{dn})/n$, where n is the number of points on the curve; T_{d1}, T_{d2}, and T_{dn} are the temperature values for each moment of time. We also found the temperature difference (ΔT_d) between Bottom Temp. and Average Temp. of the droplet at various surface temperatures (T_{surf}). Fig. 5 shows the $T_d=f(t)$ functions before and after removing the outliers.

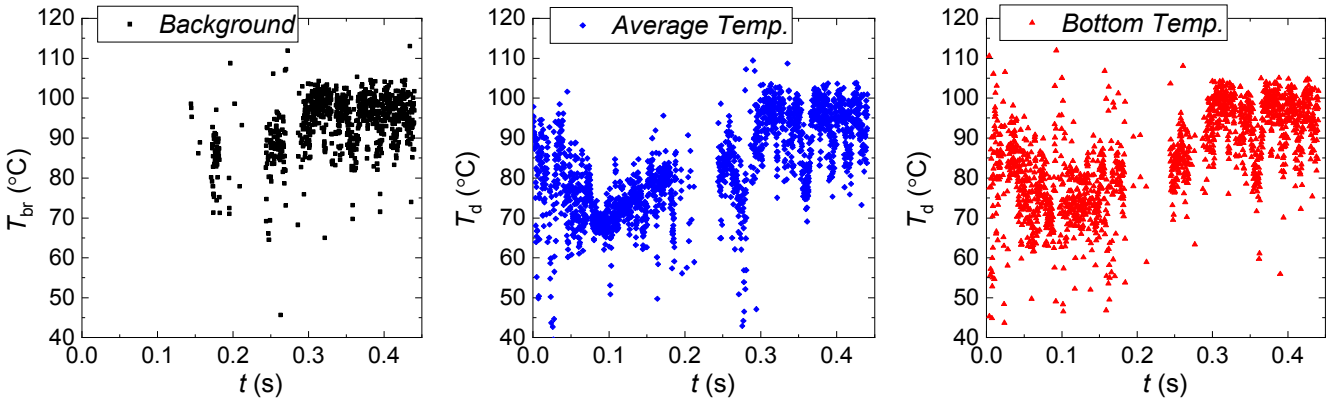

a

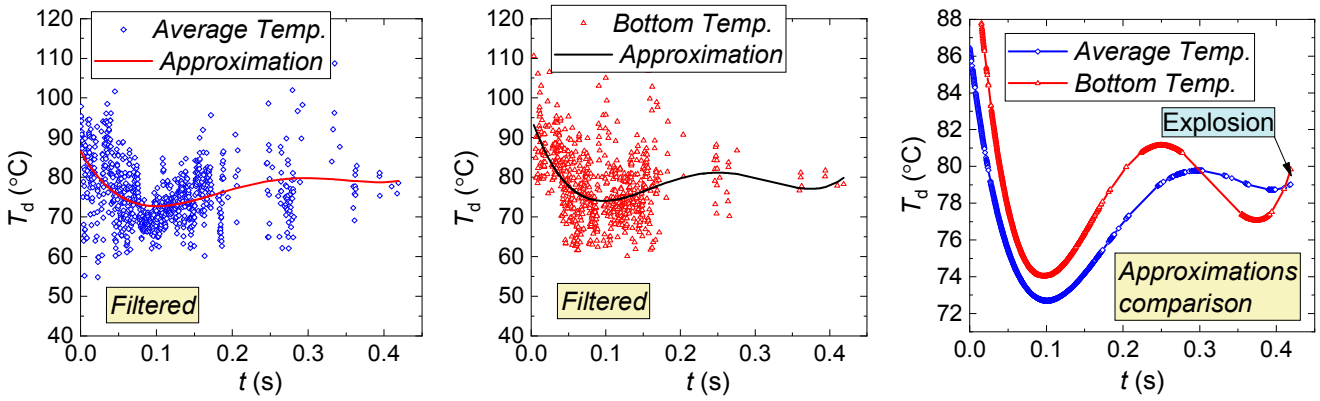

b

Fig. 5. *a* is an example temporal variation in T_d and T_{br}; *b* is the variation in the droplet temperature (Average Temp.) and the temperature of the lower droplet part (Bottom Temp.) over time after filtration and comparison of the results obtained.

Following the experiments, we obtained typical mechanisms of the explosive dispersion of heterogeneous droplets (Fig. 6). It is necessary to give a brief description of these mechanisms. When heating an emulsion droplet, we first observed micro-droplets under 50 μm in diameter forming within the mixed droplet. Then they grew in size up to 200–300 μm followed by a micro-explosion. The overall mechanism of this process corresponds to the one earlier described in [25]. In the case of an immiscible droplet, the mechanism was as follows: an initially one-piece water fragment started to split into separate droplets up to 450–500 μm in diameter. Then followed their further breakup resulting in a micro-explosion as well. Thus, immediately before the micro-explosion, the emulsion droplet and the immiscible droplet had quite a similar structure (Fig. 6).

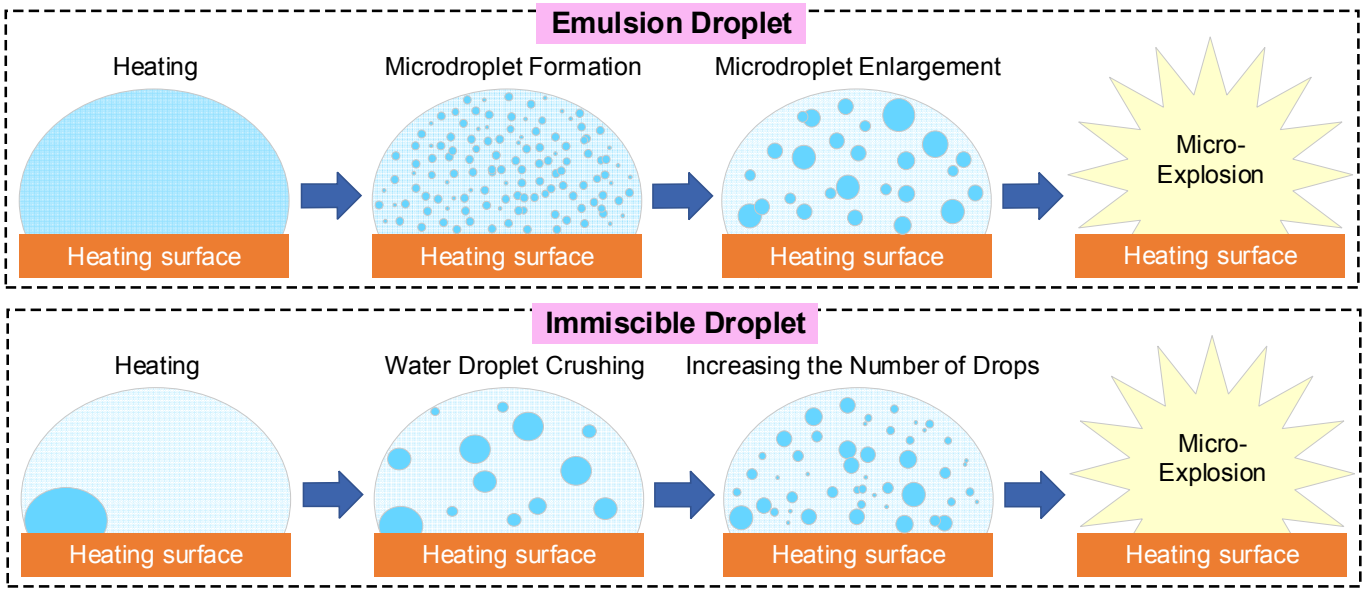

Fig. 6. Main stages of the process under study for an emulsion droplet and an immiscible droplet.

Before the experiments recording the droplet temperature, we compared the destruction times (lifetimes) of droplets (t_d) with and without Rhodamine B. Fig. 7 below shows the curves of the droplet lifetime versus the substrate temperature for an emulsion droplet and immiscible droplet. Clearly (Fig. 7), the influence of the Rhodamine B fluorophore in a droplet on its lifetime is negligible. The experiments did not show any effect of Rhodamine B on bubble nucleation in a two-component droplet.

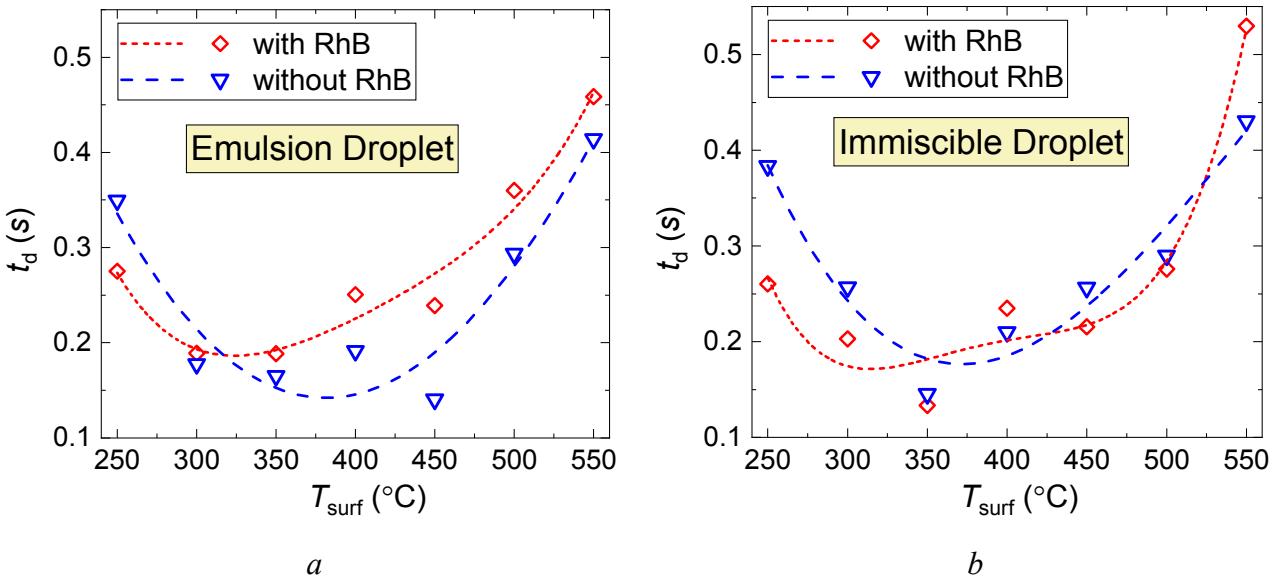

a *b*

Fig. 7. Droplet lifetime (t_d) versus substrate temperature (T_{surf}) for an emulsion droplet (*a*) and immiscible droplet (*b*)

Results and Discussion

Fig. 8 shows typical video frames and temperature fields of two-component droplets of the compositions under study while being heated (during the interval from droplet placement on a heated surface and up to its micro-explosion). Following the analysis of the obtained temperature fields (Fig. 8), we can point out two important practical aspects. First, it is possible to record the temperatures of separate micro-droplets if the size (diameter) of a droplet is at least 2-3 px. With a scale factor of 0.0285 mm/px, the minimum size of a droplet sufficient for recording its temperature is about R_d=25–50 μm. There was no difficulty in recording the temperature of larger droplets, as shown in Fig. 8. Second, in the case of an emulsion droplet, when the radius of water droplets in the main drop is several microns, all the micro-droplets are evenly distributed throughout the drop, which makes it possible to record the luminous intensity of the whole drop (Fig. 8*b*, 0.0208-0.0366 s). When the micro-droplets are becoming larger, their size (R_d) is apparently smaller than 25 μm and the concentration is insufficient for the even distribution within a tetradecane drop. At this stage, intense fluorescence is practically not observed (Fig. 8*b*, 0.1936 s). However, when micro-droplets coalesce, we manage to record the intense fluorescence and, hence, plot temperature fields (Fig. 8*b*, 0.221-0.266 s).

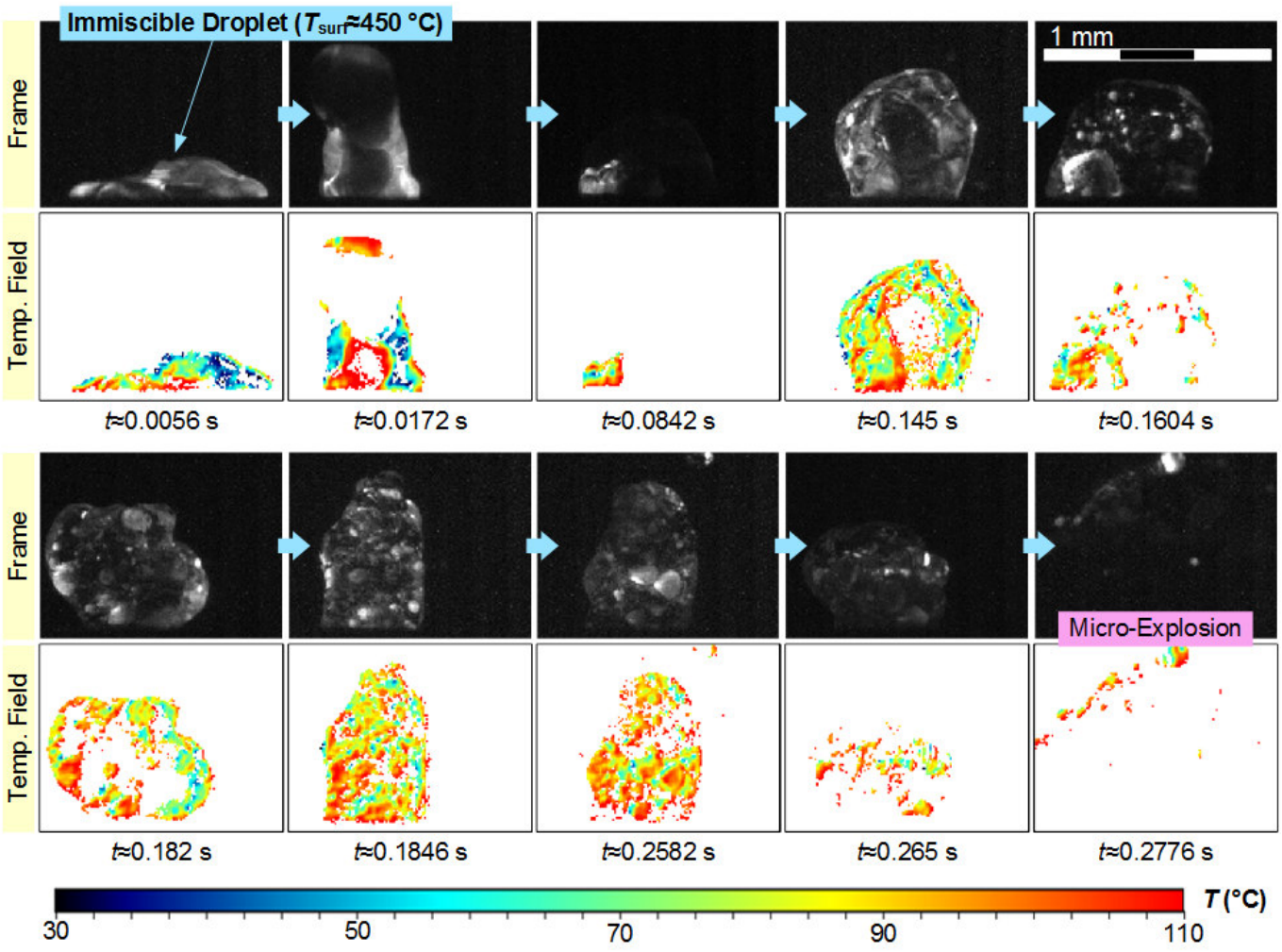
Immiscible Droplet (T_{surf}≈450 °C)
1 mm
Frame
Temp. Field
t≈0.0056 s
t≈0.0172 s
t≈0.0842 s
t≈0.145 s
t≈0.1604 s
Frame
Micro-Explosion
Temp. Field
t≈0.182 s
t≈0.1846 s
t≈0.2582 s
t≈0.265 s
t≈0.2776 s
T (°C)
30
50
70
90
110

a

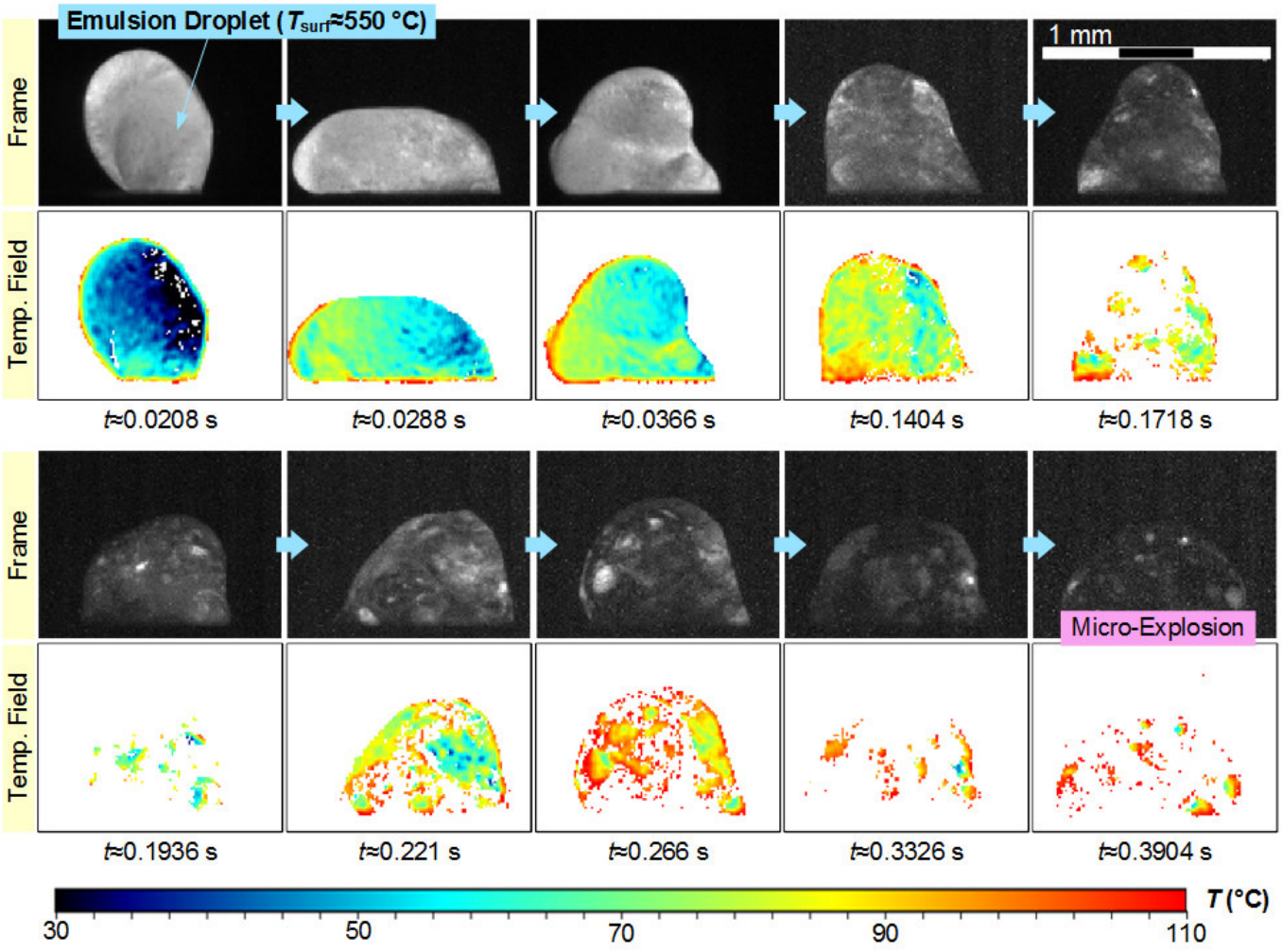

b

Fig. 8. Video frames of droplets and corresponding temperature fields obtained using 2-Color LIF in the *micro-explosion* regime: *a* – immiscible droplet (T_{surf}≈450 °C); *b* – emulsion droplet (T_{surf}≈550 °C).

When considering the experimental results, we analyzed the possibility of morphology dependent resonances (MDRs) or lasing effect. This phenomenon usually manifests itself either with small droplets (with a radius of under 50 μm) or with relatively high specific power of the laser radiation source [42-44]. The specific radiation power in the experiments approximated 3.5 W/cm^2, and the size of the minimum recorded separate droplets (as mentioned before) was Rd=25–50 μm. Such parameters, according to Ref. [43], indicate the minimization of the laser resonance inside micro-droplets and, thus, of the temperature measurement error. At the same time, an emulsion droplet consists of water micro-droplets evenly distributed in tetradecane, which is generally similar to a micro-spray cloud analyzed in Ref. [42]. Ref. [42] also shows that there can be areas of nonphysical temperatures caused by multiply scattered light in a micro-spray, usually in its periphery. In our experiments, we did not observe any areas of nonphysical temperatures, which indicates the visible absence of MDRs or lasing effects.

Figs. 9 and 10 present typical variations in Average Temp. and Bottom Temp. with varying heating surface temperatures for an emulsion droplet and an immiscible droplet. The analysis of the results obtained leads to the following important points. First, the droplet temperature in its lower part

(Bottom Temp.) was 3–8 °C higher than the average droplet temperature (Average Temp.) in all the experiments and almost throughout the heating process. Second, the temperature of an emulsion droplet changed more gradually than that of an immiscible droplet. The latter must be related to the uneven water distribution within the combustible component for an immiscible droplet, *i.e.*, the presence of a clear core.

Despite the general patterns of the growing droplet temperature over time observed in the research (Figs. 9, 10), the heating and destruction of heterogeneous fuel-water droplets is accompanied by constant intermixing, disruption, and coalescence of micro-droplets, as well as occasional droplet jumping on the heating surface. Selective evaporation of two-component fuel-water droplets is not ruled out either, i.e., either water or hydrocarbon evaporates first [45]. In experiment #1, for instance, the emulsion droplet had the temperature T_{surf}≈500 °C (Fig. 9). Due to the droplet jumping on the substrate, the droplet temperature T_d started decreasing 0.09 s from the droplet placement on the substrate and only retained its value at t≈0.24 s.

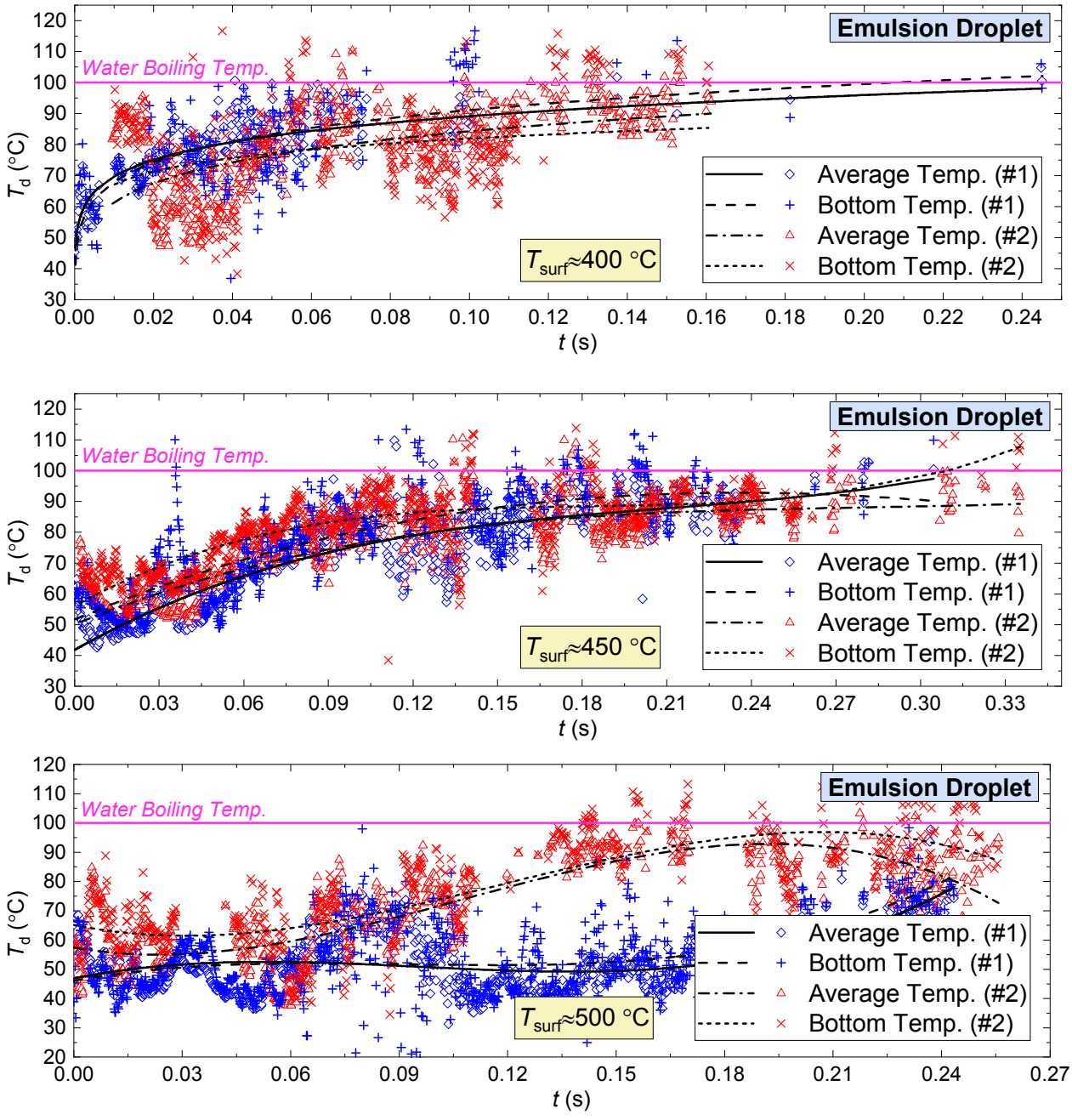

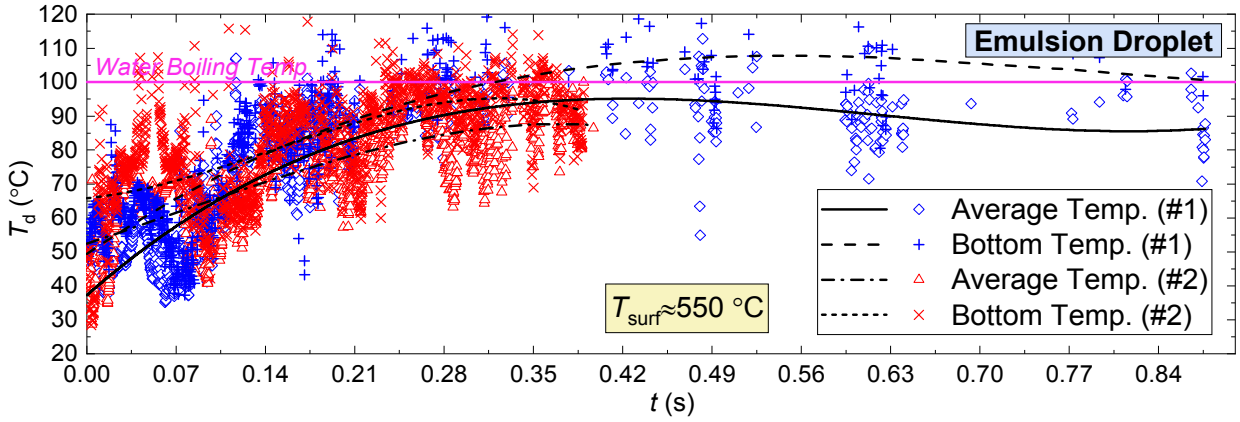

Fig. 9. Dynamics of the temporal T_d variations (Average Temp. and Bottom Temp.) for an *emulsion droplet* with varying heating surface temperature (T_{surf}=400–550 °C) in the *micro-explosion* regime (#1, #2 are the numbers of experiments).

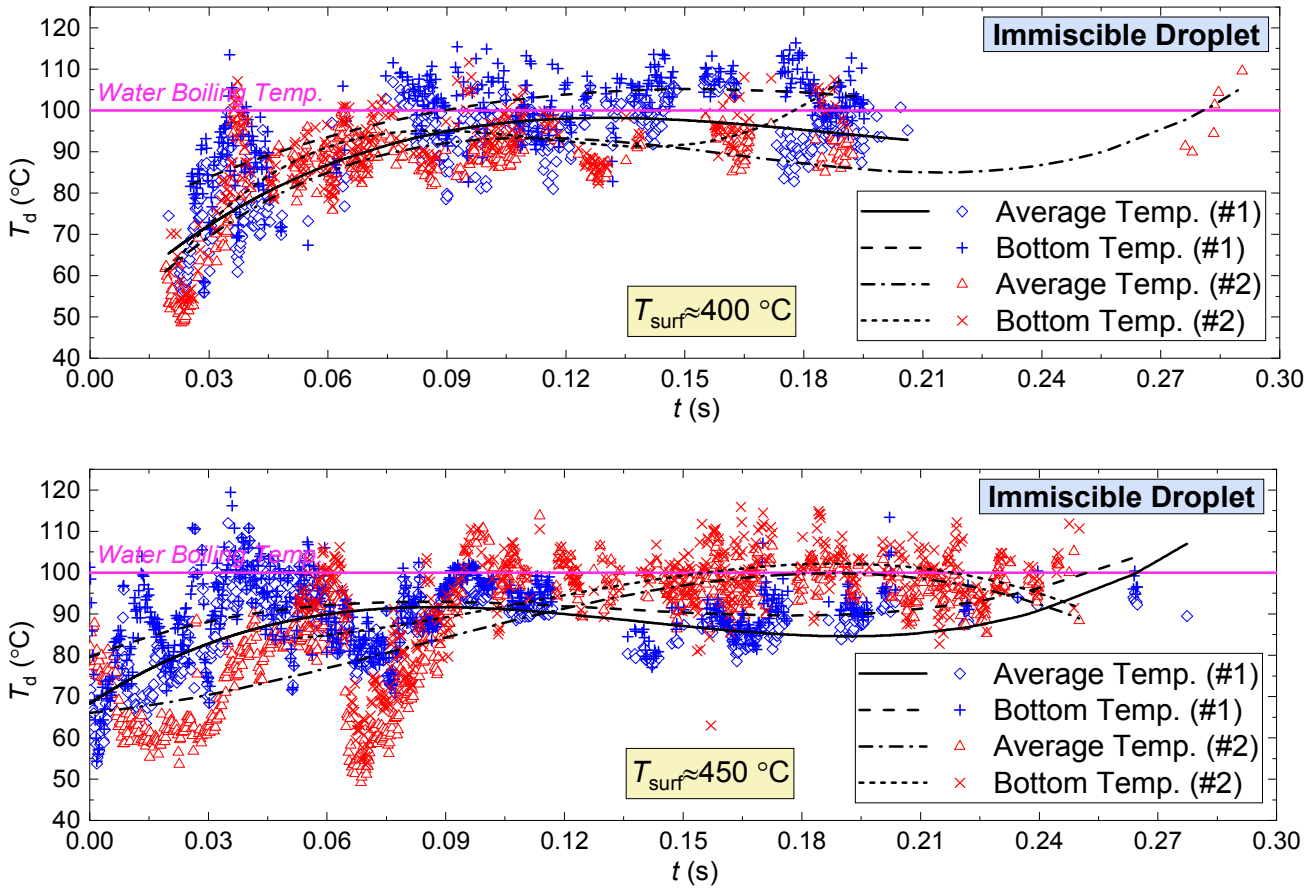

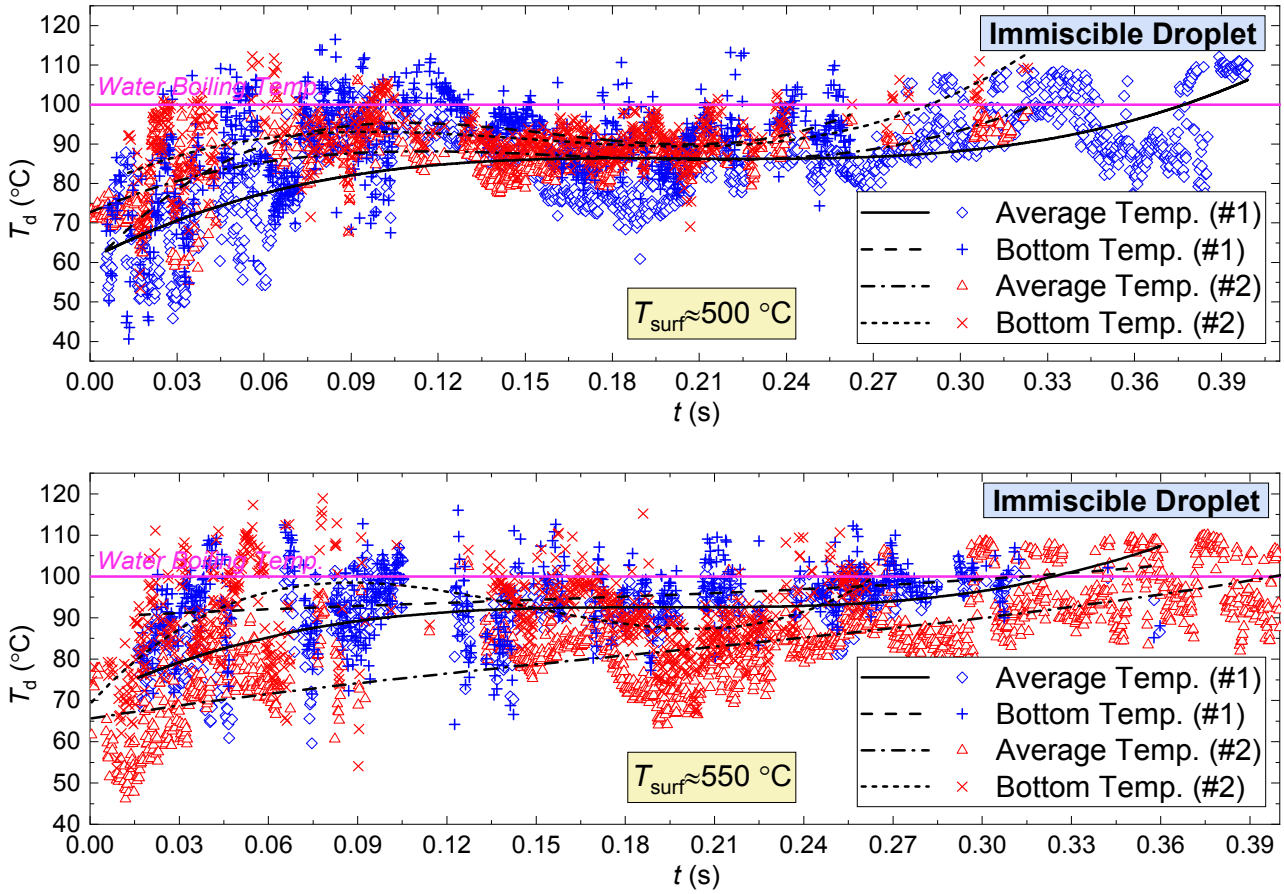

Fig. 10. Dynamics of the temporal T_d variations (Average Temp. and Bottom Temp.) for an *immiscible droplet* with varying heating surface temperature (T_{surf}=400–550 °C) in the *micro-explosion* regime (#1, #2 are the numbers of experiments).

The findings presented in Figs. 9 and 10 show that the micro-explosion of a droplet occurs when the temperature of water in it (as a rule, Average Temp.) reaches about 100 °C. The initial temperature varied within the range of 30–50 °C in this experiment. At the same time, the temperature remains stable from 0.03 s to 0.2 s before the micro-explosion. The times of temperature stabilization differ because when a droplet reaches the boiling temperature (100 °C), it starts to move actively on the substrate and jump up. This is a random process continuing until the micro-explosive fragmentation. It is also established that the values of Bottom Temp. are always higher than Average Temp. throughout the droplet heating.

Fig. 11*a* shows the temporal variation in the difference between Bottom Temp. and Average Temp. of an immiscible droplet. It was given by $\Delta T_d = T_{BT} - T_{AT}$, where T_{BT} and T_{AT} are Bottom Temp. and Average Temp. at each moment of time, respectively. The analysis of the results (Fig. 11*a*) shows that ΔT_d normally approaches zero at the starting moment, when a droplet hits the substrate. In other words, no significant heating of any part of the droplet is observed. Then, in the interval of 0.02–0.05 s, the ΔT_d rises up to 35–40 °C. After a marked extremum, there is a decrease in ΔT_d related to droplet heating. However, even while the droplet is being heated, there are local ΔT_d extrema, both above and below zero. The latter apparently stems from the liquid layers mixing in the droplet as well as the droplet jumping

occasionally on the heated surface. In all the experiments considered, ΔT_d almost always took on a near-zero value immediately before the micro-explosive breakup of the droplet (Fig. 11*b*). Thus, we cannot positively claim that a certain local value of ΔT_d provides the micro-explosion regime (*i.e.*, is enough for this process). It is only by analyzing the long-term dynamics of ΔT_d variation and the fitting curve shape (Fig. 11) that we can speak of the moment preceding the droplet breakup. A number of functional relationships can be used to approximate the data presented in Fig. 11*a*. However, when presenting the measurements, our task was to note the general trend of the ΔT_d reduction from the start of droplet heating until its destruction. Having analyzed all the data and tried various fitting curves for histograms similar to the one in Fig. 11*a* (because there are usually several extrema), we decided to use a third order polynomial as an approximating function.

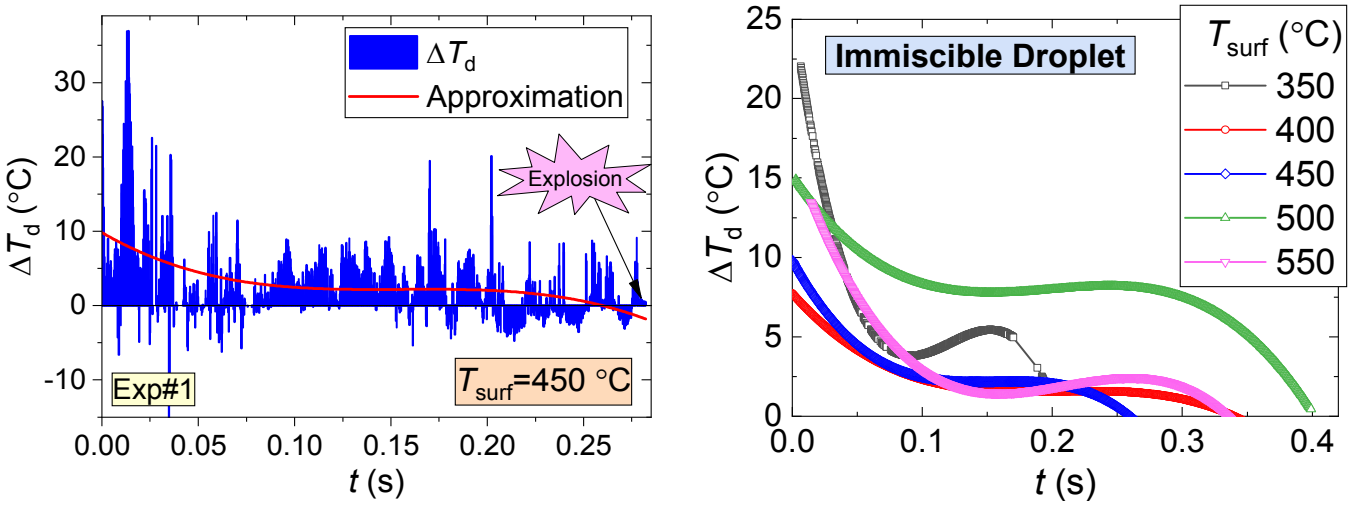

a *b*

Fig. 11. Dynamics of variation in the difference (ΔT_d) between Bottom Temp. and Average Temp. of an *immiscible droplet* with heating surface temperature (T_{surf}≈450 °C) in the *micro-explosion* regime (*a*), $\Delta T_d = f(T_{surf})$ for different heating surface temperature (*b*).

Figs. 12, 13 show the functions of the mean values of the difference (ΔT_d) between Bottom Temp. and Average Temp. of an emulsion droplet and an immiscible droplet. Due to the abrupt changes in the instantaneous values of ΔT_d (Fig. 11), we used the mean value of ΔT_d for the whole droplet heating stage to evaluate the patterns in the process being analyzed. The mean value of ΔT_d is given by $\Delta T_d = ((T_{BT1}-T_{AT1})+(T_{BT2}-T_{AT2})+\ldots+(T_{BTn}-T_{ATn}))/n$, where T_{BT} and T_{AT} are the instantaneous values of Bottom Temp. and Average Temp. at each moment of time, respectively. We considered two schemes:

— Scheme #1. The negative values of ΔT_d were disregarded;

— Scheme #2. All the ΔT_d values were accounted for in the calculation.

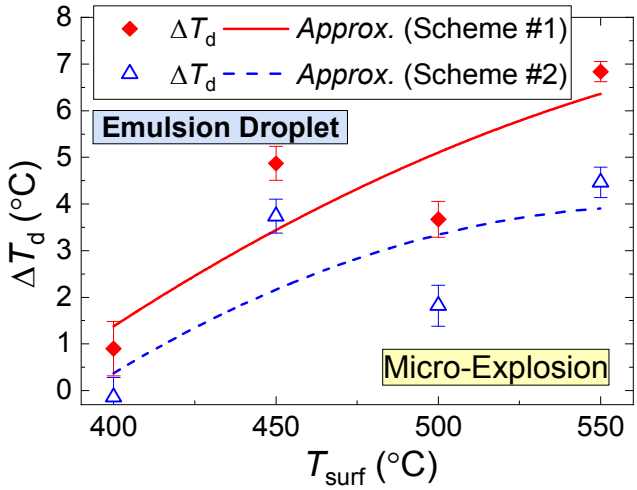

Fig. 12. Mean difference (ΔT_d) between Bottom Temp. and Average Temp. of an *emulsion droplet* with varying heating surface temperature (T_{surf}) in the *micro-explosion* regime.

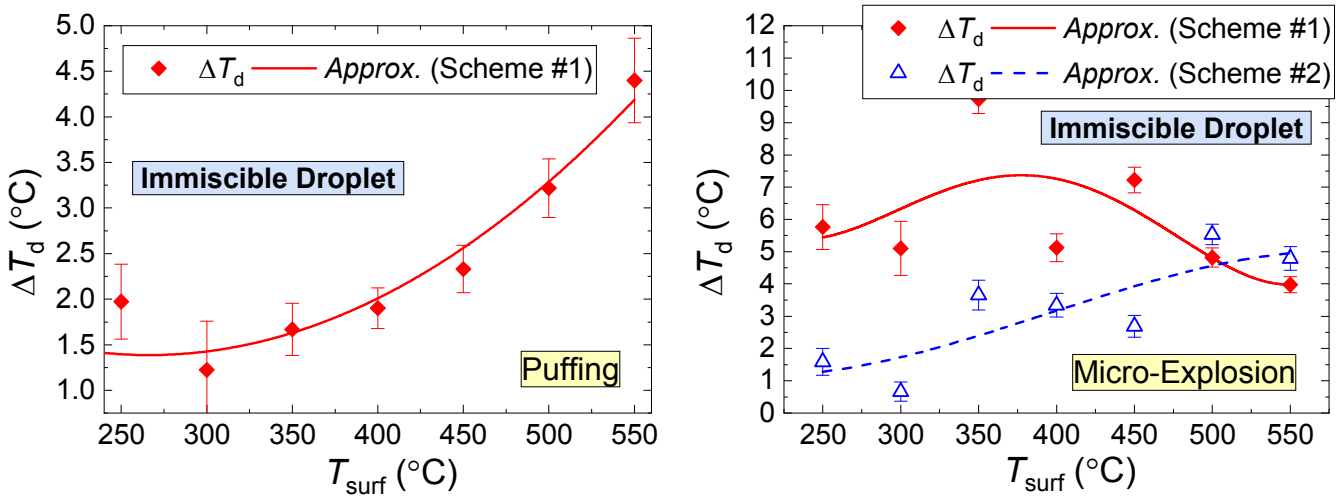

Fig. 13. Mean difference (ΔT_d) between Bottom Temp. and Average Temp. of an *immiscible droplet* with varying heating surface temperature (T_{surf}) in the *micro-explosion* and *puffing* regimes.

Clearly (Figs. 12, 13), when Scheme #2 is used, the $\Delta T_d = f(T_{surf})$ curves have a smoother increasing shape as compared to Scheme #1. Presumably, the removal of negative ΔT_d values has an adverse effect on the result.

When analyzing the results obtained, we calculated the heating rates of droplets under study in a similar way as in [17]. The instantaneous and mean heating rates were given by the following equations.

Average heating rate throughout the process:

$$W_h = T_{AT}/t_d,$$

where T_{AT} is the mean value of Average Temp. throughout the heating time and t_d is the droplet lifetime.

Instantaneous heating rate within a selected short time interval:

$$W_h = \Delta T_{AT}/\Delta t,$$

where ΔT_{AT} is the variation in the mean value of Average Temp. over Δt; Δt is the time interval taken as 0.01 s in the calculations.

Figs. 14 and 15 show the smoothed instantaneous and mean values of W_h for an emulsion droplet and an immiscible droplet. Clearly, the instantaneous W_h values decrease almost throughout the heating process. Local maximums and minimums are still observed but they mostly result from the droplet jumping on the heating surface (as in the results of experiment #1 for emulsion droplet at T_{surf}≈500 °C (Fig. 9)). At the same time, the character and values of W_h on the curves (Figs. 14*a*, 15*a*) do not allow us to draw firm conclusions about the effect of T_{surf} on the heating rates. The mean values of W_h decrease with an increase in T_{surf} (Figs. 14*b*, 15*b*). At the same time, the heating rate of an immiscible droplet is significantly (200–230 °C) higher than the same parameter of an emulsion droplet at T_{surf}=400 °C. At T_{surf}≥450 °C, the heating rates of the two droplet types under study do not differ by more than 40–50 °C/s.

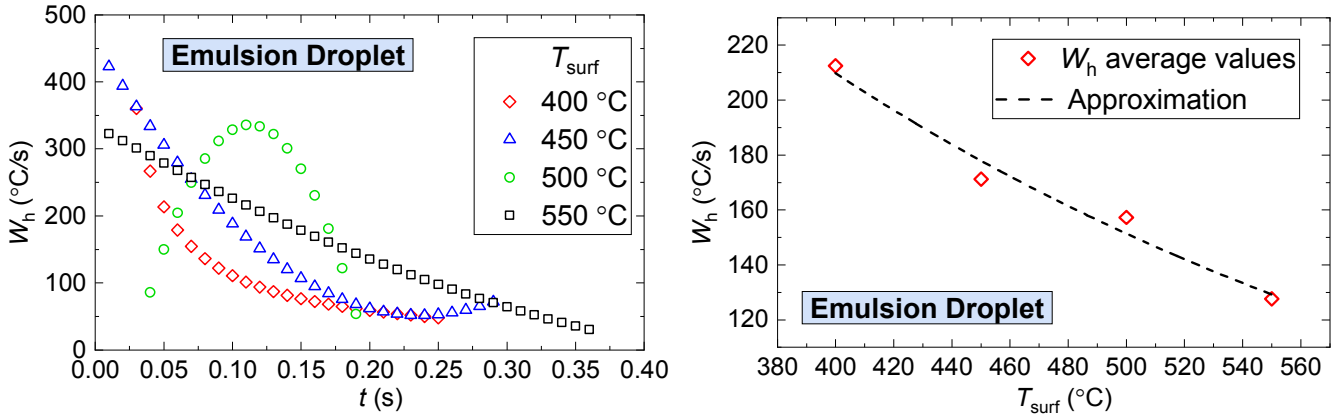

a *b*

Fig. 14. Temporal variation dynamics of the instantaneous heating rates of an *emulsion droplet* with varying heating surface temperature (T_{surf}=400–550 °C) in the *micro-explosion* regime (*a*), as well as the average heating rate versus the surface temperature (T_{surf}) (*b*).

To explain the shape of the W_h=*f*(T_{surf}) curves obtained (Figs. 14*b*, 15*b*), we calculated the mean breakup times of the droplet types under study. The results are shown in Fig. 16. You can see that the times t_d were decreasing within the T_{surf}=150–350 °C range. Their decrease is rather sharp until 250°C, which corresponds to the boiling point of tetradecane; after this value of temperature, we can suppose that the heat flux between the plate and the drop is no longer increasing. In the range T_{surf}=350–550 °C, however, the droplet lifetimes increased non-linearly in the range of 0.2 to 0.6 s. At the same time, the t_d growth trend is typical of both emulsion droplets and immiscible droplets in the *micro-explosion* and *puffing* regimes.

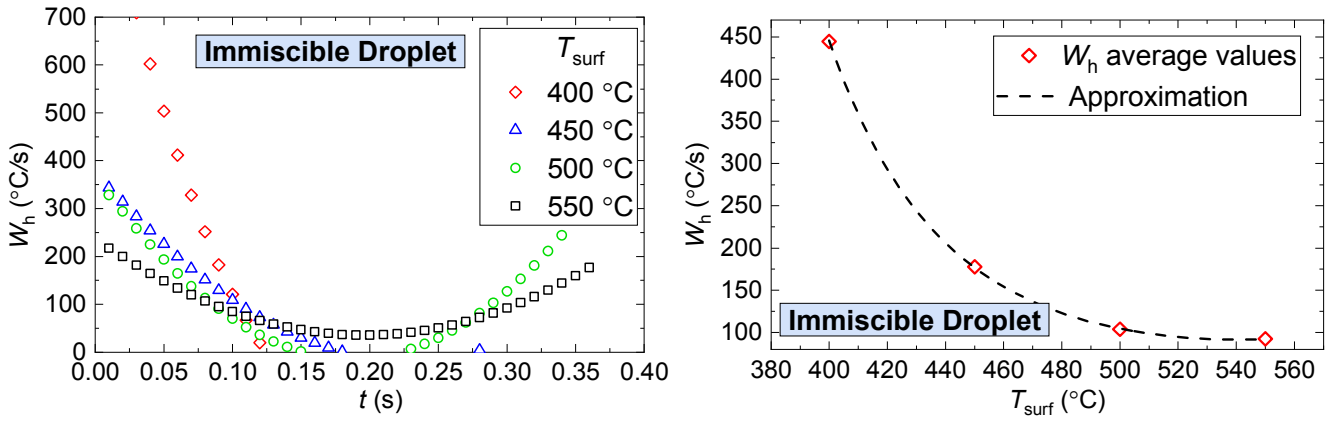

a *b*

Fig. 15. Temporal variation dynamics of the instantaneous heating rates of an *immiscible droplet* with varying heating surface temperature (T_{surf}=400–550 °C) in the *micro-explosion regime* (*a*), as well as the average heating rate versus the surface temperature (T_{surf}) (*b*).

An increase in the t_d stems from the droplet jumping on the substrate. As a result, the droplet was not in direct contact with the heated surface, hence a longer time was required to trigger of the explosive breakup (Fig. 16). For this reason, the average liquid droplet heating rates (W_h) increase with an increase in T_{surf} (Figs. 14*b*, 15*b*).

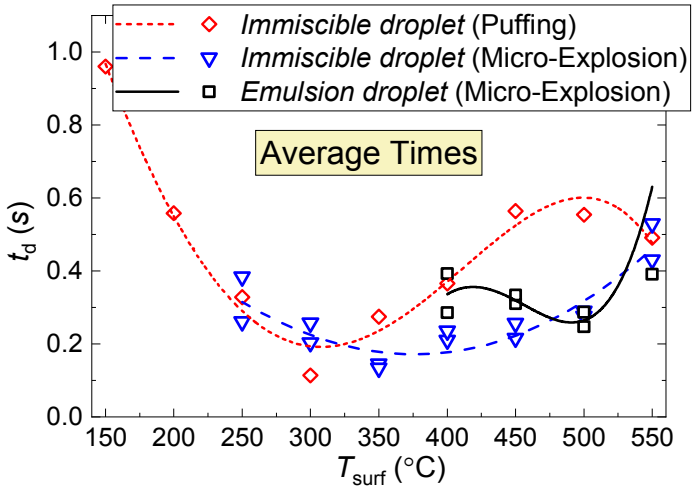

Fig. 16. Aligned curves of the average droplet breakup times (t_d) versus the heating surface temperature (T_{surf}) for an *immiscible droplet* in the *micro-explosion* and *puffing* regimes and an *emulsion droplet* in the *micro-explosion* regime.

Conclusion

(i) The experiments with mixed and immiscible droplets allowed us to specify principal differences in the mechanisms of their micro-explosive fragmentation. The video frames showed that water micro-droplets within the emulsion actively coalesced and, therefore, formed rather large liquid fragments. They were the basis for bubble nucleation and further growth. In the case of a two-component droplet, the reverse processes were recorded, *i.e.*, a large water core broke up within a fuel droplet. Vapor

bubbles were formed at the surface of these fragments and coalesced later on. When these bubbles reached critical pressures, droplets broke up into fragments. These findings indicate that the growth of vapor bubbles is intensified when water micro-droplets within a fuel droplet reach the average size of 50 to 100 μm. For the bubbles to reach this average critical size in a two-component droplet, the water core atomization was needed, and in the case of emulsion, the coalescence of water micro-droplets.

(ii) At the heating stage, the temperature differences in two-component droplets were much lower than in an emulsion droplet due to the uneven water distribution in a droplet. Here the temperature difference could range from 1°C to 10 °C. The droplet temperature in the puffing regime was on average 1–3 °C higher than in the micro-explosion regime at the same heating temperatures. This happened because a droplet remained on the substrate for a longer time in the puffing regime: 0.05–0.25 s longer than an emulsion droplet.

(iii) The difference (ΔT_d) between the Bottom Temp. and the Average Temp. of a two-component droplet grew 1–5 °C higher with an increase in the surface temperature (T_{surf}) irrespective of the droplet breakup regime (explosion or puffing). For an emulsion droplet, this range was 1–7 °C.

The future work is devoted to a comparison of the integral characteristics of secondary fragments formed during a micro-explosion. In particular, their quantity, sizes, kinetic energy, temperature, surface area will be determined. The decisive influence on them is exerted by the initial state of the drop – an emulsion or two unmixed components, as well as the temperature of the heated surface.

Acknowledgments

The work on the paper was supported by the National Research Tomsk Polytechnic University (project VIU-ISHFVP-60/2019) (contributions by Pavel Strizhak), (project VIU-ISHFVP-184/2019) (contributions by Roman Volkov) and by the Région Pays de la Loire: Chaire Connect Talent ODE (contributions by Omar Moussa, Dominique Tarlet, Jérôme Bellettre).

References

1. Yu. Varaksin, Fluid Dynamics and Thermal Physics of Two Phase Flows: Problems and Achievements, Heat mass transf. phys. gas dynam. 51 (3) (2013) 377–407. https://doi.org/10.1134/S0018151X13030073
2. S.S. Sazhin, A.E. Elwardany, P.A. Krutitskii, V. Deprédurand, G. Castanet, F. Lemoine, E.M. Sazhina, M.R. Heikal, Multi-component droplet heating and evaporation: Numerical simulation versus experimental data, Int. J. Therm. Sci. 50 (2011) 1164–1180. https://doi.org/10.1016/j.ijthermalsci.2011.02.020
3. C.A. Hernández-Bocanegra, A.H. Castillejos, F.A. Acosta-Gonzalez, X.X. Zhou, B.G. Thomas, Measurement of heat flux in dense air-mist cooling: Part I – A novel steady-state technique,

Experimental Therm. Fluid Sci. 44 (2013) 147–160. https://doi.org/10.1016/j.expthermflusci.2012.06.015

4. Yu.P. Sosnin, Contact water heaters, Moscow, Stroyizdat Publ. (1974). [in Russian].
5. P.A. Strizhak, R.S. Volkov, The integral characteristics of the deceleration and entrainment of water droplets by the counter flow of high-temperature combustion products, Exp. Therm. Fluid Sci. 75 (2016) 54–65. https://doi.org/10.1016/j.expthermflusci.2016.01.018
6. R.S. Volkov, P.A. Strizhak, Planar laser-induced fluorescence diagnostics of water droplets heating and evaporation at high-temperature, Appl. Therm. Eng. 127 (2017) 141-156. https://doi.org/10.1016/j.applthermaleng.2017.08.040
7. Zh.-F. Zhou, M.-Y. Hu, H. Xin, B. Chen, G.-X. Wang, Experimental and theoretical studies on the droplet temperature behavior of R407C two-phase flashing spray, Int. J. Heat Mass Transf. 136 (2019) 664–673. https://doi.org/10.1016/j.ijheatmasstransfer.2019.03.042
8. J. Linden, Laser Induced Phosphor Thermometry - Feasibility and precision in combustion applications. Lund University (2012).
9. A. Khalid, K. Kontis, Thermographic phosphors for high temperature measurements: principles, current state of the art and recent applications, Sensors 8 (9) (2008) 5673–5744. https://doi.org/10.3390/s8095673
10. G. Särner, M. Richter, M. Aldén, Two-dimensional thermometry using temperature-induced line shifts of ZnO:Zn and ZnO:Ga fluorescence, Opt. Lett. 33 (2008) 1327-1329. https://doi.org/10.1364/OL.33.001327
11. A. Omrane, S. Santesson, M. Aldéna, S. Nilsson, Laser techniques in acoustically levitated micro droplets, Lab. Chip. 4 (2004) 287-291. https://doi.org/10.1039/B402440K
12. A. Charogiannis, F. Beyrau, Laser induced phosphorescence imaging for the investigation of evaporating liquid flows, Exp. Fluid. (2013) 54:1518. https://doi.org/10.1007/s00348-013-1518-2
13. C. Abram, M. Pougin, F. Beyrau, Temperature field measurements in liquids using ZnO thermographic phosphor tracer particles, Exp. Fluids 57 (2016) 115. https://doi.org/10.1007/s00348-016-2200-2
14. J. Brübach, A. Patt, A. Dreizler, Spray thermometry using thermographic phosphors, Appl. Phys. B 83 (2006) 499–502. https://doi.org/10.1007/s00340-006-2244-8
15. C. Abram, B. Fond, F. Beyrau, Temperature measurement techniques for gas and liquid flows using thermographic phosphor tracer particles, Prog. Energy Comb. Sci. 64 (2018) 93-156. https://doi.org/10.1016/j.pecs.2017.09.001
16. R.S. Volkov, P.A. Strizhak, Measuring the temperature of a rapidly evaporating water droplet by Planar Laser Induced Fluorescence, Meas. 135 (2019) 231–243. https://doi.org/10.1016/j.measurement.2018.11.047

17. G.V. Kuznetsov, M.V. Piskunov, R.S. Volkov, P.A. Strizhak, Unsteady temperature fields of evaporating water droplets exposed to conductive, convective and radiative heating, Appl. Therm. Eng. 131 (2018) 340–355. https://doi.org/10.1016/j.applthermaleng.2017.12.021
18. R. Volkov, P. Strizhak, Measurement of the temperature of water solutions, emulsions, and slurries droplets using planar-laser-induced fluorescence, Meas. Sci. Technol. 31 (2020) 035201. https://doi.org/10.1088/1361-6501/ab56cf
19. P.A. Strizhak, R.S. Volkov, G. Castanet, F. Lemoine, O. Rybdylova, S.S. Sazhin, Heating and evaporation of suspended water droplets: Experimental studies and modelling, Int. J. Heat Mass Transf. 127 (2018) 92-106. https://doi.org/10.1016/j.ijheatmasstransfer.2018.06.103
20. P. Lavieille, F. Lemoine, G. Lavergne, J.F. Virepinte, M. Lebouche, Temperature measurements on droplets in monodisperse stream using laser-induced fluorescence, Exp. Fluids 29 (2000) 429-437. https://doi.org/10.1007/s003480000109.
21. G. Castanet, A. Labergue, F. Lemoine, Internal temperature distributions of interacting and vaporizing droplets, Int. J. Therm. Sci. 50 (2011) 1181-1190. https://doi.org/10.1016/j.ijthermalsci.2011.02.001
22. A. Charogiannis, J.S. An, C.N. Markides, A simultaneous planar laser-induced fluorescence, particle image velocimetry and particle tracking velocimetry technique for the investigation of thin liquid-film flows, Exp. Therm. Fluid Sci. 68 (2015) 516-536. https://doi.org/10.1016/j.expthermflusci.2015.06.008
23. Y.N. Mishra, F.A. Nada, S. Polster, E. Kristensson, E. Berrocal, Thermometry in aqueous solutions and sprays using two-color LIF and structured illumination, Opt. Express 24 (2016) 4949-4963. https://doi.org/10.1364/OE.24.004949
24. B. Peterson, E. Baum, B. Böhm, V. Sick, A. Dreizler, Spray-induced temperature stratification dynamics in a gasoline direct-injection engine, Proc. Combust. Inst. 35 (2015) 2923-2931. https://doi.org/10.1016/j.proci.2014.06.103
25. O. Moussa, D. Francelino, D. Tarlet, P. Massoli, J. Bellettre, Insight of a water-in-oil emulsion drop under Leidenfrost heating using laser-induced fluorescence optical diagnostics, At. Sprays. 29 (2019) 1-17. https://doi.org/10.1615/AtomizSpr.2019029233
26. Y. Suzuki, T. Harada, H. Watanabe, M. Shoji, Y. Matsushita, H. Aoki, T. Miura, Visualization of aggregation process of dispersed water droplets and the effect of aggregation on secondary atomization of emulsified fuel droplets, Proc. Combust. Inst. 33 (2011) 2063-2070. https://doi.org/10.1016/j.proci.2010.05.115
27. J. Shinjo, J. Xia, L.C. Ganippa, A. Megaritis, Physics of puffing and micro-explosion of emulsion fuel droplets, Phys. Fluids 26 (2014) 103-302. https://doi.org/10.1063/1.4897918

28. H. Watanabe, T. Harada, Y. Matsushita, H. Aoki, T. Miura, The characteristics of puffing of the carbonated emulsified fuels, Int. J. Heat Mass Transf. 52 (2009) 3676-3684. https://doi.org/10.1016/j.ijheatmasstransfer.2009.02.033
29. O. Moussa, D. Tarlet, P. Massoli, J. Bellettre, Investigation on the conditions leading to the micro-explosion of emulsified fuel droplet using two colors LIF method, Exp. Therm. Fluid Sci. 116 (2020) 110106. https://doi.org/10.1016/j.expthermflusci.2020.110106
30. L. Wang, J. Wang, X. Qiao, D. Ju, Z. Lin, Effect of ambient temperature on the micro-explosion characteristics of soybean oil droplet: The phenomenon of evaporation induced vapor cloud, Int. J. Heat Mass Transf. 139 (2019) 736–746. https://doi.org/10.1016/j.ijheatmasstransfer.2019.04.038
31. Z. Nissar, O. Rybdylova, S.S. Sazhin, M. Heikal, A. Rashid B.A. Aziz, M.A. Ismael, A model for puffing/microexplosions in water/fuel emulsion droplets, Int. J. Heat Mass Transf. 149 (2020) 119208. https://doi.org/10.1016/j.ijheatmasstransfer.2019.119208
32. B. Kichatov, A. Korshunov, A. Kiverin, A. Saveliev, The role of explosive boiling in the process of foamed emulsion combustion, Int. J. Heat Mass Transf. 119 (2018) 199–207. https://doi.org/10.1016/j.ijheatmasstransfer.2017.11.116
33. D. Tarlet, E. Mura, C. Josset, J. Bellettre, C. Allouis, P. Massoli, Distribution of thermal energy of child-droplets issued from an optimal micro-explosion, Int. J. Heat Mass Transf. 77 (2014) 1043–1054. https://doi.org/10.1016/j.ijheatmasstransfer.2014.06.054
34. D. Tarlet, C. Josset, J. Bellettre, Comparison between unique and coalesced water drops in micro-explosions scanned by differential calorimetry, Int. J. Heat Mass Transf. 95 (2016) 689–692. https://doi.org/10.1016/j.ijheatmasstransfer.2015.12.054
35. D. Tarlet, C. Allouis, J. Bellettre, The balance between surface and kinetic energies within an optimal micro-explosion, Int. J. Therm. Sci. 107 (2016) 179–183. https://doi.org/10.1016/j.ijthermalsci.2016.04.008
36. R.S. Volkov, P.A. Strizhak, Using Planar Laser Induced Fluorescence to explore the mechanism of the explosive disintegration of water emulsion droplets exposed to intense heating, Int. J. Therm. Sci. 127 (2018) 126-141. https://doi.org/10.1016/j.ijthermalsci.2018.01.027
37. D.V. Antonov, P.A. Strizhak, Heating, evaporation, fragmentation, and breakup of multi-component liquid droplets when heated in air flow, Chem. Eng. Res. Des. 146 (2019) 22-35. https://doi.org/10.1016/j.cherd.2019.03.037
38. D.V. Antonov, R.M. Fedorenko, P.A. Strizhak, Child droplets produced by micro-explosion and puffing of two-component droplets, Appl. Therm. Eng. 164 (2020) 114501. https://doi.org/10.1016/j.applthermaleng.2019.114501
39. D.V. Antonov, M.V. Piskunov, P.A. Strizhak, Explosive disintegration of two-component drops under intense conductive, convective, and radiant heating, Appl. Therm. Eng. 152 (2019) 409-419. https://doi.org/10.1016/j.applthermaleng.2019.02.099

40. D. Antonov, M. Piskunov, P. Strizhak, D. Tarlet, J. Bellettre, Dispersed phase structure and micro-explosion behavior under different schemes of water-fuel droplets heating, Fuel 259 (2020) 116241. https://doi.org/10.1016/j.fuel.2019.116241
41. C. Cen, H. Wu, C. Lee, L. Fan, F. Liu, Experimental investigation on the sputtering and micro-explosion of emulsion fuel droplets during impact on a heated surface, Int. J. Heat Mass Transf. 132 (2019) 130–137. https://doi.org/10.1016/j.ijheatmasstransfer.2018.12.007
42. J. Palmer, M.A. Reddemann, V. Kirsch, R. Kneer, Development steps of 2-color laser-induced fluorescence with MDR-enhanced energy transfer for instantaneous planar temperature measurement of micro-droplets and sprays. ILASS Europe, 28th Annual Conference on Liquid Atomization and Spray Systems, Valencia, Spain (2017). http://dx.doi.org/10.4995/ILASS2017.2017.4591
43. J. Palmer, M.A. Reddemann, V. Kirsch, R. Kneer, Applying 2D-2cLIF-EET thermometry for micro-droplet internal temperature imaging. Exp. Fluids 59 (2018) 51. https://doi.org/10.1007/s00348-018-2506-3
44. J. Palmer, L. Schumacher, M.A. Reddemann, V. Kirsch, R. Kneer, Applicability of pulsed 2cLIF-EET for micro-droplet internal thermometry under evaporation conditions, Exp. Fluids 61 (2020) 99. https://doi.org/10.1007/s00348-020-2935-7
45. C.T.Avedisian, M.Fatehi, An experimental study of the Leidenfrost evaporation characteristics of emulsified liquid droplets, Int. J. Heat Mass Transf. 31 (1988) 1587-1603. https://doi.org/10.1016/0017-9310(88)90271-2